Modification of spontaneous emission from nanodiamond colour centres on a structured surface

New Journal of Physics
The open-access journal for physics

Modification of spontaneous emission from nanodiamond colour centres on a structured surface

F A Inam[1,2], T Gaebel[1,2], C Bradac[1,2], L Stewart[2,3], M J Withford[1,2,3], J M Dawes[2,3], J R Rabeau[1,2,4,5] and M J Steel[1,2,3,5]

[1] Centre for Quantum Science and Technology, Department of Physics and Astronomy, Macquarie University, Sydney, NSW 2109, Australia
[2] MQ Photonics Research Centre, Department of Physics and Astronomy, Macquarie University, Sydney, NSW 2109, Australia
[3] ARC Centre of Excellence for Ultrahigh-bandwidth Devices for Optical Systems (CUDOS), Department of Physics and Astronomy, Macquarie University, Sydney, NSW 2109, Australia
[4] ARC Centre of Excellence for Engineered Quantum Systems (EQUS), Department of Physics and Astronomy, Macquarie University, Sydney, NSW 2109, Australia
E-mail: james.rabeau@mq.edu.au and michael.steel@mq.edu.au

New Journal of Physics **13** (2011) 073012 (20pp)
Received 31 January 2011
Published 11 July 2011
Online at http://www.njp.org/
doi:10.1088/1367-2630/13/7/073012

Abstract. Colour centres in diamond are promising candidates as a platform for quantum technologies and biomedical imaging based on spins and/or photons. Controlling the emission properties of colour centres in diamond is a key requirement for the development of efficient single-photon sources having high collection efficiency. A number of groups have achieved an enhancement in the emission rate over narrow wavelength ranges by coupling single emitters in nanodiamond crystals to resonant electromagnetic structures. In this paper, we characterize in detail the spontaneous emission rates of nitrogen-vacancy centres at various locations on a structured substrate. We found a factor of 1.5 average enhancement of the total emission rate when nanodiamonds are on an opal photonic crystal surface, and observed changes in the lifetime distribution. We present a model for explaining these observations and associate the lifetime properties with dipole orientation and polarization effects.

[5] Authors to whom any correspondence should be addressed.

Contents

1. Introduction

In order to meet some of the demanding requirements for optical quantum technologies, bright sources of single photons [1–5] are required. Colour centres in diamond nanocrystals are among the leading candidates to fill this need, owing to a host of attractive properties including room-temperature photostability and convenient spin polarization by optical pumping. However, existing realizations are far from ideal—intrinsic spontaneous emission lifetimes in the range of 1–30 ns combined with the problem of maximizing the collection efficiency of emitted photons limit the total number of collected photons. In addition, at least for the most widely studied nitrogen-vacancy (NV) centre, the intrinsic emission spectrum is very broad. Consequently, several groups are nowadays developing techniques for enhancing both the emission rate and photon collection efficiency, as well as for manipulating the spectral shape.

A variety of approaches have been explored, mostly based on the idea of changing the local electromagnetic environment seen by the emitted photons. One class of methods involves coupling the radiating dipole to a single strongly localized mode of a high-Q resonator such as a microsphere [6, 7], microdisc [8] or photonic crystal cavity [9–12], enhancing the emission rate through the Purcell effect [13, 14]. Alternatively, using a solid immersion lens for the collection of NV emission, the brightness may be increased significantly without affecting the local electromagnetic environment [15, 16]. However, as mentioned, a key challenge of diamond colour centres, as compared with other systems such as quantum dots, is the linewidth of the intrinsic emission spectrum. For the NV centre, the overall linewidth is of the order of 200 nm with the zero phonon line (ZPL) at 637 nm having a width of several nm at room temperature [17, 18]. By contrast, the cavity linewidth of a typical photonic crystal cavity with a Q of 10^4 is over an order of magnitude smaller than the width of the ZPL. Therefore, while the rate of emission within the cavity line can increase markedly, this represents a small fraction of the total emitted power. So the primary effect of coupling the centre to a cavity mode is a reshaping of the emission spectrum, with little increase in the overall rate of emitted photons.

An additional increase in the cavity Q increases the local emission rate further, but also reduces the frequency range over which enhancement occurs by the same factor. Some improvements are possible: under cryogenic conditions, the width of the ZPL does narrow [19] and therefore a slightly stronger effect is expected. Alternatively, one could use other centres such as the nickel-related [20–24] group, chromium [25–27] and silicon centres [28] that have narrower intrinsic spectra (although again still broader than the cavity linewidth); however, the fabrication and spectroscopy of these centres are still not as mature as for NV centres.

Consequently, there is merit in pursuing complementary schemes that enhance the emission rate over a broad spectral band at the expense of very strong enhancement for a single wavelength. One recent example exploited the very large local electric fields associated with localized surface plasmons to achieve an enhancement in the overall emission rate of an NV centre by a factor as large as 14 [29, 30]. We recently showed less pronounced but broadband suppression of the emission rate by embedding nanodiamonds in regular three-dimensional (3D) photonic crystals [9].

For the most part, these considerations are applicable to emission by a single centre with a given orientation for its electric dipole moment and a given nanodiamond size. If an ensemble of measurements is considered, the situation becomes more complicated as there is variation in the emission rate from centre to centre associated with nanodiamond size and shape [31], as well as the orientation of the centre dipole with respect to the local electromagnetic environment (i.e. the refractive index distribution). The relative importance of these different contributions depends on the type of structure with which the nanodiamond colour centre is interacting: for example, a flat interface or structured surface [32]. A recent work reported on the lifetime distributions of NV centres in disordered scattering media [33]. The lifetime distribution of NV centres in nanodiamond crystals was measured on a coverslip surrounded by air and, subsequently, by a droplet of water, and a small reduction in the mean lifetime was observed. Finally, the nanodiamond crystals were surrounded by high-refractive-index dielectric spheres of size around 250 nm and a lengthening in the fluorescence lifetime was observed, which was attributed to a reduction in the local density of states (LDOS).

In this work, we theoretically and experimentally study the emission of single NV centres placed on flat dielectric substrates and on a structured opal photonic crystal surface. We consider the statistics of lifetimes associated with size, shape and orientation and measure a 1.5-fold reduction in the overall lifetime of single NV centres on the surface of the opal. The enhancement is interpreted in terms of an averaging of the polarization dependence of the emission rate associated with the structured surface. The rest of this paper is organized as follows. In section 2, we review the theory of dipole emission rates in structured dielectric environments based on the LDOS and discuss issues peculiar to NV nanodiamonds. The experimental details, from sample preparation to the characterization and lifetime measurement of single NV centres, are described in section 3. The emission rate calculations are presented and compared with experimental results in section 4. Section 5 presents a discussion of the sensitivity of the calculations with respect to non-idealities in the nanodiamonds, and section 6 presents the conclusions.

2. Theoretical background of emission rates in structured dielectrics

We begin by recalling the treatment of emission in structured environments and discussing issues related to NV nanodiamonds. In the weak coupling regime that applies in this work,

the spontaneous emission rate Γ of a dipole at a position $\mathbf{r}$ is determined by Fermi's golden rule applied to electric dipole transitions [34]:

$$\Gamma = \frac{1}{\tau} = \frac{\pi\omega}{\hbar}\mu^2 \sum_{\mathbf{k},\sigma} |\hat{\mathbf{d}} \cdot \mathbf{E}_{\mathbf{k},\sigma}(\mathbf{r})|^2 \delta(\omega - \omega_{\mathbf{k},\sigma}), \tag{1}$$

where τ is the spontaneous emission lifetime, ω is the transition frequency, $\boldsymbol{\mu} = \mu\,\hat{\mathbf{d}}$ is the relevant dipole moment matrix element and the sum is taken over all possible emitted photon modes $(\mathbf{k}, \sigma)$ labelled by wavevector and polarization. The modes have local electric field profiles $\mathbf{E}_{\mathbf{k},\sigma}(\mathbf{r})$. In particular, the rate is influenced by the dielectric environment through the electromagnetic LDOS [35–37]

$$\rho(\omega, \mathbf{r}) = \sum_{\mathbf{k},\sigma} |\hat{\mathbf{d}} \cdot \mathbf{E}_{\mathbf{k},\sigma}(\mathbf{r})|^2\, \delta(\omega - \omega_{\mathbf{k},\sigma}). \tag{2}$$

The LDOS accounts for both the local field intensity of the available modes and the relative orientation of the dipole with respect to the field of each mode. The LDOS itself is a purely classical quantity that can be found from the electromagnetic Green tensor and so relative emission rates can be found from classical electromagnetic calculations. This exact picture encompasses a variety of systems. At one extreme is emission enhancement by coupling to a single high-Q cavity mode of large field amplitude and small mode volume. At the other extreme of a dipole embedded in a homogeneous medium, the dipole couples to a continuum of modes. The emission rate is then proportional to the refractive index n with an n^3 increase in the density of modes outweighing a reduction in the electric field intensity of n^2, so that

$$\Gamma(n) = n\Gamma_0, \tag{3}$$

where Γ_0 is the emission rate of the dipole in free space. (Here we neglect an atomic-scale local field factor which can be regarded as a constant since the NV centre is locally surrounded by the same diamond lattice whether we consider bulk or nanodiamond [38, 39].) For both these extremes, the dipole orientation plays a trivial role, with a cosine factor in the case of a single cavity mode, and no dependence at all for a homogeneous medium.

In contrast, the emission rate of dipoles near non-uniform but non-resonant structures is affected by both the distribution of photonic modes and the dipole orientation. This set of structures is exactly the class that may help in inducing broadband enhancement of dipole emission. The simplest example is a linear dipole on or near a flat dielectric surface, a system that has been studied in detail for many years [40, 41]. In this case, the emission rate is determined by interference between directly emitted waves and those reflected from the surface. The relative emission rate as a function of distance from the interface is shown in figure 1 for parallel and perpendicular dipole orientations and for two different substrate refractive indices. There is a strong dependence on the dipole orientation through the polarization dependence of the Fresnel reflection coefficients. (How to deal with the fact that NV is actually a 2D rather than a linear dipole is discussed in section 4.2.)

2.1. Local dielectric environment

The emission of NV centres in nanodiamonds is commonly characterized for crystals deposited on a glass substrate [40, 42], and in the first part of our experiments described below we also make such measurements. The nanodiamond on a substrate might seem to correspond to the

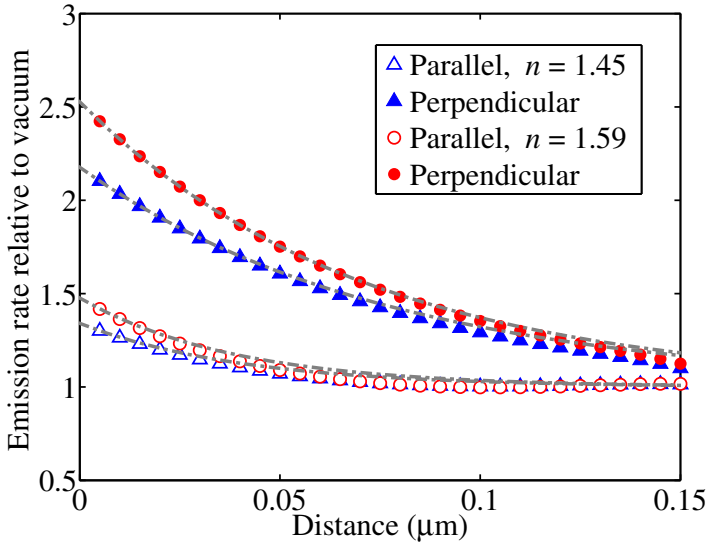

Figure 1. Relative emission rate for radiating dipoles near an interface between two dielectrics, corresponding to parallel and perpendicular dipole orientations relative to the interface, for an emission wavelength of 680 nm. The dashed lines represent the semi-analytical theory in [40]. The symbols are exact FDTD results. The small discrepancy at large distances is due to an approximation in the analytic theory. Curves are labelled according to the relative index constant $n = n_2/n_1$.

geometry just described of a dipole near a surface. In fact, several reports in the diamond literature [40, 42] have invoked an even simpler scalar picture for this problem, arguing that the dipole effectively emits into two half-spaces (air and substrate,) each of which promotes emission at the rate $n/(\mathrm{n_d}\tau_\mathrm{b})$, according to equation (3). Here $n_\mathrm{d} \approx 2.4$ is the refractive index of diamond and $\tau_\mathrm{b} = 11.6$ ns is the accepted spontaneous emission lifetime for an NV centre in bulk diamond. Therefore the resulting lifetime should be approximately given by the expression [42]

$$\tau_\mathrm{sub} = \frac{\tau_\mathrm{b}}{((1-f_\mathrm{s})/n_\mathrm{d}) + (n_\mathrm{s} f_\mathrm{s}/n_\mathrm{d})}, \tag{4}$$

where f_s is the volume fraction of the substrate and n_s is the substrate index. For a planar interface, we set $f_\mathrm{s} = 1/2$. This expression does agree quite well with the measured mean lifetime of around 23 ns [40, 42]. More generally, for an arbitrary volume fraction f_s, equation (4) describes a diamond embedded in a non-planar two-component structure. Figure 2 shows the lifetimes predicted by equation (4) for a number of substrate materials. Naturally, as the dipole emitter becomes more enveloped in material, its lifetime decreases. While this ignores interference effects and dipole orientation, it provides some context for our subsequent more rigorous results.

However, while the argument leading to equation (4) is reasonable for an isolated dipole such as a dye molecule close to a surface, it is not appropriate for a dipole trapped inside a high-index sub-wavelength particle, such as an NV centre in a nanodiamond with diameter $a < 100$ nm. It has long been known that for such nanoparticle-embedded emitters, where the

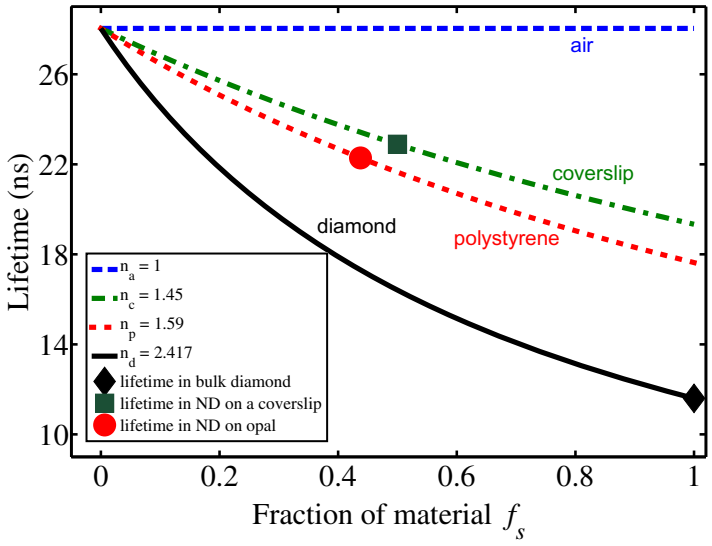

Figure 2. Lifetime for a single NV centre as a function of the volume fraction of high-index material in its surroundings for several relevant materials [42]. The circle, square and diamond symbols show the lifetimes of the NV centres on opal and coverslip substrates inside a nanodiamond (ND) crystal and in bulk diamond, respectively.

emission wavelength λ is larger than that of the particle, the emission rate Γ_p is expected to be suppressed compared with the rate Γ_b in a macroscopic piece of the same material [31, 33, 38, 43]. For a spherical particle in the limit $\lambda \gg a$, the suppression ratio tends to

$$\frac{\Gamma_p}{\Gamma_b} = \frac{1}{\varepsilon}\left(\frac{3}{\varepsilon+2}\right)^2 \approx 0.062, \tag{5}$$

where $\varepsilon = n_d^2$. The treatment of Chew [31] shows that suppression is essentially a local field effect at the particle scale with the electric field inside the nanodiamond reduced by the Lorentz–Lorenz factor $3/(\varepsilon+2)$. (This is distinct from the atomic-scale local field effect the dipole experiences owing to the diamond crystal lattice structure [44]. As mentioned earlier, since in both bulk diamond and nanodiamond the NV centre is embedded in a diamond lattice, we expect the atomic local field factor to remain unchanged.) Emission suppression in small particles has been clearly demonstrated for dye molecules in polystyrene spheres by Schniepp and Sandoghdar [43]. At least for a spherical particle [31], the emission rate depends very weakly on the precise position and orientation of the dipole inside the particle. For non-spherical particles, some dependence on orientation leading to a broadening of the linewidth distribution is expected [39, 45]. We show in section 5 that this is a minor effect in our systems.

It follows from this discussion that a correct theory of emission from a colour centre within a nanodiamond on any kind of substrate, whether planar or otherwise, must explicitly incorporate the influence of the diamond material making up the nanoparticle as well as the surrounding environment. Moreover, the dependence on orientation and position from the interface as suggested by figure 1 indicates that a much more sophisticated treatment than equation (4) is required in order to fully understand the emission behaviour. The fact that equation (4) gives the observed value of approximately 23 ns for nanodiamonds on a coverslip

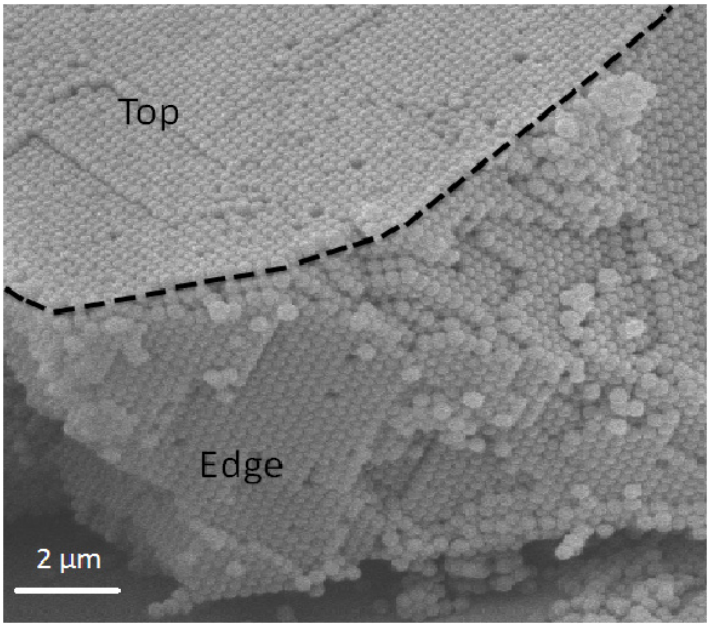

Figure 3. SEM image of the opal photonic crystal composed of polystyrene ($n = 1.59$) microspheres of diameter 320 nm.

must therefore be regarded as a coincidence, rather than as an accurate picture of the radiation physics. A full treatment seems to be uncommon in the literature and complicates the calculation as we will discuss in the next section. Ruijgrok *et al* [33] report having performed finite-difference time-domain (FDTD) simulations but do not provide the details.

2.2. Structured surfaces

In the second part of our experimental study, we consider emission from diamond nanocrystals placed on the surface of an opal photonic crystal composed of polystyrene spheres with refractive index 1.59 (see figure 3). An opal photonic crystal consists of a regular 3D arrangement of microspheres in a face-centred cubic structure [46, 47]. We have previously demonstrated emission suppression for nanodiamonds embedded *within* an opal photonic crystal with a stop band tuned to the NV emission band [9]. In this work, we concentrate on the change in emission rates due to the structured surface of the opal rather than through photonic band gap effects.

Specifically, nanodiamonds placed on the opal surface can be positioned on the apex of a polystyrene bead or in an interstitial position between three microspheres, providing a range of interaction conditions depending on the surrounding environment. The fraction of the nearby space occupied by the high-index material varies from site to site, but just as importantly, so does the relative orientation of adjacent surfaces. In particular, for a nanocrystal positioned in an interstitial site, the distinction between parallel and perpendicular orientations to nearby boundaries is much less pronounced than for the flat surface (see figure 4) and we might expect some averaging of these two extremes with a net increase in emission rate. We show below that this is true and that the predicted and measured increases considerably exceed the change that would be predicted based only on the variation in the material volume fraction that follows from figure 2.

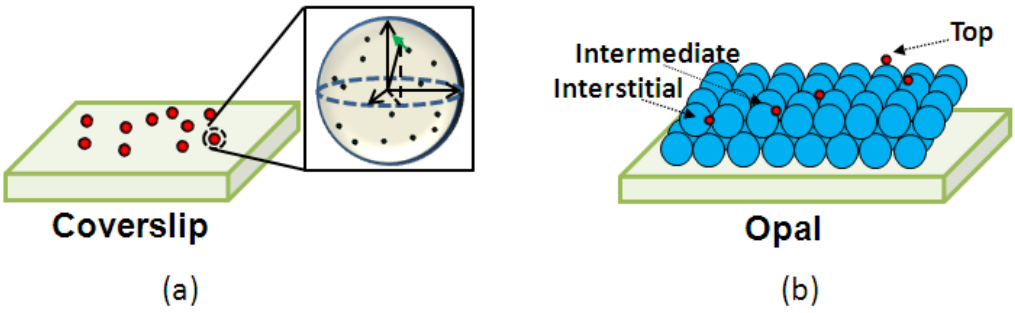

Figure 4. Schematic representation of nanodiamond positions on (a) the coverslip and (b) the opal layer that were experimentally and computationally studied. The inset shows some of the possible random positions (dots) of the dipole inside the diamond sphere as well as a possible random orientation of an individual dipole (arrow).

3. Experimental details

We now describe our experiments, including the preparation of nanodiamond doped substrate samples and the lifetime measurements.

3.1. Sample preparation

Coverslips of thickness $(150 \pm 20)\,\mu$m were etched in piranha acid solution (H_2SO_4/H_2O_2, 3 : 1) and dried in a dry nitrogen flow. Opal films were grown using the controlled evaporation method [48] as follows. A coverslip was placed in a scintillation vial containing a 10 ml solution of polystyrene microspheres of $(0.320 \pm 0.016)\,\mu$m diameter (Bangs Laboratories) diluted by ultrapure water. The refractive index of the microspheres was specified to be $n_p = 1.59$. Dilutions of 0.1% weight of polystyrene were used. The vial was then placed in a temperature-controlled oven set to 40 °C [9]. Coverslip and opal samples were prepared by pipetting a 100 μl ethanol suspension of diamond nanocrystals (containing 7 mg of diamond nanocrystals per ml) over each surface and allowing it to dry. These diamonds were previously analysed by atomic force microscopy [49, 50] and found to have a mean size of 54 nm and a distribution of 30–80 nm. Nanodiamonds deposited on the opal were imaged using scanning electron microscopy (SEM) in order to assess the typical distribution of nanodiamonds over the opal surface. Of the 365 nanodiamonds analysed, $f_T = 10\%$ of the particles tended to be located on the top of a bead, $f_I = 65\%$ were in the interstitial position and the remaining $f_R = 25\%$ were distributed in various other locations in between the top and the interstitial position (see figure 4(b)).

3.2. Lifetime measurements

A 100 mW continuous wave laser (Coherent Compass; $\sim$300 μW incident on the sample) operating at 532 nm was used to optically excite luminescence from the NV centres. The laser was focused through the back surface of the coverslip and onto the sample using a 100 $\times$ infinity-corrected oil immersion objective with a numerical aperture of 1.3 (Olympus)

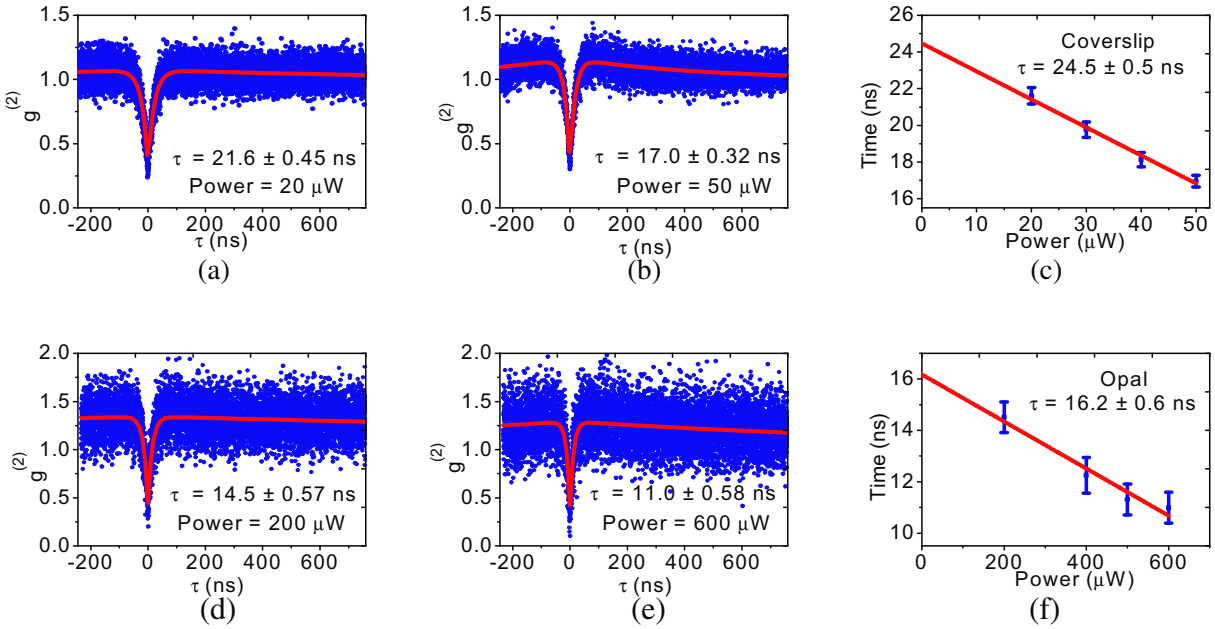

Figure 5. (a, b, d and e) Typical background corrected [42] second-order correlation measurements (blue) and fit (red) to a three-level system [18] to obtain decay times for different excitation powers. (c, f) Lifetime as a function of input power. The final lifetime value was obtained by extrapolating the decay time to vanishing excitation power [18]. The error bars in the figure correspond to a 95% confidence interval from the three-level fitting of the $g^{(2)}$ curve.

and luminescence was collected confocally through a pinhole. The diamond was excited at normal incidence to the ⟨111⟩ plane of the opal, which naturally grows parallel to the substrate. A spectrometer (Acton) with a cooled CCD camera (Princeton Instruments) was used to characterize the luminescence, and a Hanbury Brown and Twiss (HBT) interferometer with single-photon-sensitive avalanche photodiodes (PerkinElmer SPCM-AQR-14) was used to measure the photon statistics. Photon counting and correlation was carried out using a time-correlated single-photon-counting module (PicoHarp 300, PicoQuant GmbH). To eliminate the complication of multiple NV lifetimes in a single crystal, we identified diamonds with single NV centres by measuring the second-order correlation function $g^{(2)}$ using the HBT setup. A dip in the $g^{(2)}$ curve below 50% of the maximum value indicates a single centre as seen in figures 5(a), (b), (d) and (e). Contrast below 100% is due to the background signal (reflection of the laser or emission from a nearby centre) [42]. On the basis of our previous characterizations [49], less than 1% of the nanodiamonds used in these experiments are expected to contain single NV centres. In this case, we identified a total of $N_C = 37$ single centres on the coverslip and $N_O = 27$ single centres on the opal. Unfortunately, the opal surface does not appear in our confocal images, so we could not identify the specific environment (top, interstitial and others) of each individual centre. In our calculations below, we assume that they are distributed with similar statistics to the full set of 365 nanodiamonds observed with the SEM, as described in section 3.1.

NV centre lifetimes were determined using the power dependence of second-order correlation ($g^{(2)}$) traces. For each single NV centre, raw coincidence traces $c(t)$ were collected

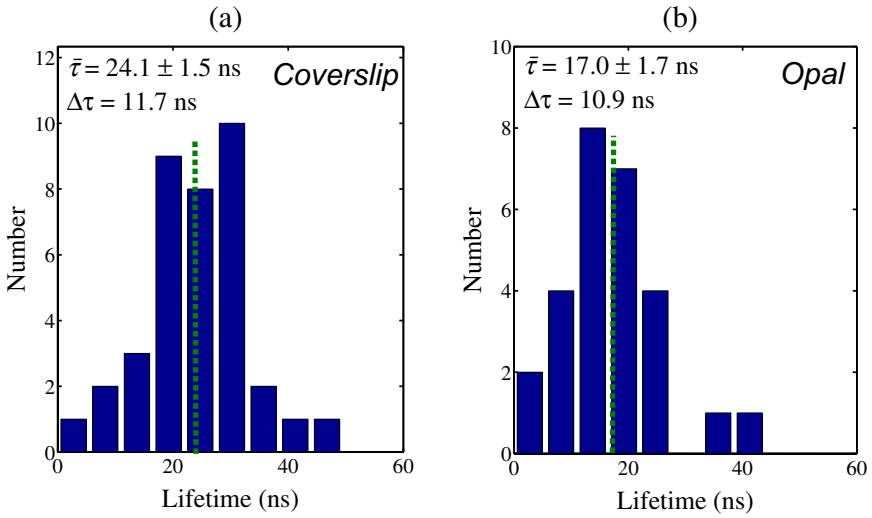

Figure 6. Experimental distribution of the NV centre lifetime on a coverslip (a) and on an opal (b). Dotted lines denote the mean value. Quoted values are mean lifetime $\bar{\tau}$ and the range $\Delta\tau$ that contains 50% of the centres.

over a range of laser powers. The correlation data $c(t)$ were then normalized and background corrected to obtain the correlation function $g^{(2)}$ in the following standard way [42]. The raw coincidence rate $c(t)$ counted during a time T and within time bin width w was first normalized to that of a Poissonian source according to the formula $C_N(\tau) = c(\tau)/(\mathrm{N}_1 N_2 w T)$, where $N_{1,2}$ are the count rates of each detector. This was then corrected for the background signal to yield the correlation function as $g^{(2)}(\tau) = [C_N(\tau) - (1-\rho^2)/\rho^2$, where $\rho = (\mathrm{S}_1 + S_2)/((\mathrm{S}_1 + S_2) + (\mathrm{B}_1 + B_2))$ is the signal-to-background ratio and $S_{1,2}$ and $B_{1,2}$ are the signal and background counts on each detector. The $g^{(2)}$ correlation traces (see figures 5(a), (b), (d) and (e)) were fitted to a standard three-level model for the optical transition to obtain the decay times for the transitions corresponding to different excitation powers. The lifetime of the NV centre was then inferred by extrapolating the value of the decay time to vanishing excitation power [18, 42] (figures 5(c) and (f)). The errors quoted in figure 5 for the individual decay times correspond to 95% confidence limits. Note that the powers indicated in figure 5 are input powers and the much larger values for the opal are due to the need to excite the NV centre through the opal substrate. The collected photon counts and thus the excitation power at the site of the nanodiamond were of the same order for both the coverslip and the opal.

The measured lifetime distributions are shown in figure 6. The mean lifetime for the diamonds on a coverslip was (24.1 ± 1.5) ns and that for diamonds on an opal was (17.0 ± 1.7) ns (uncertainties are standard errors of the mean). As a representation of the distribution width, in figure 6 we also provide the range $\Delta\tau$ containing the middle 50% of measured lifetimes. The change from the coverslip to the opal produced a lifetime reduction of $\Delta\tau = (7.1 \pm 3.2)$ ns. To quantify the difference in the distributions, we performed a Kolmogorov–Smirnov test [51] and found that the probability that the two sample distributions come from the same underlying distribution was less than 1%.

4. Emission rate calculations

We now present a model for the emission rate distributions for the coverslip and opal geometries. Although spontaneous emission is an explicitly quantum process, the emission rate relative to a reference system can be found by classical electromagnetic calculations since the dependence on the environment is expressed through the classical LDOS (see equation (2)). We note that this analysis only accounts for radiative processes, and does not include any non-radiative contributions to the spontaneous emission lifetime. We return to this point in section 5. For each geometry discussed above, NV emission rates relative to the rate in bulk diamond were calculated using 3D FDTD simulation as follows.

4.1. Method and geometry

The dipole was considered to be enclosed in a spherical nanodiamond crystal with a diameter $D = 54$ nm. (We discuss the sensitivity of our results to shape and size of the nanodiamond in section 5.) The nanodiamond was placed in contact with either a glass substrate or part of the opal surface. The index of the glass coverslip was 1.45. The radius of the opal spheres was $a = 160$ nm and the refractive index was 1.59. For a given dipole position and orientation within the nanosphere, the electromagnetic field was excited by a sinusoidal point current source driven at a frequency $\nu = c/\lambda$ for $\lambda = 680$ nm, which is near the peak of the NV emission. Once the field configuration reached the steady state, which takes only a few optical periods as the reflected fields are weak, the power P radiated by the dipole was calculated by two methods—finding the work done by the dipole $W = \langle \mathbf{J}(t) \cdot \mathbf{E}(t) \rangle$ averaged over one optical cycle and integrating the time-averaged Poynting flux $\mathbf{S} = \langle \mathbf{E}(t) \times \mathbf{H}(t) \rangle$ over the surface of a rectangular box enclosing the dipole. The calculation was then repeated with the same dipole orientation in a uniform medium of index $n_\mathrm{d} = 2.4$ to obtain the emitted power P_b corresponding to NV emission in bulk diamond. The radiative spontaneous emission rate enhancement was then found to be $R = P/P_\mathrm{b}$.

The calculations were performed with a spatial grid of $\Delta x = 5$ nm, for which the two methods of calculating radiated power were in close agreement with each other. The total domain dimensions were 300 nm on one side for the coverslip and 700 nm for the opal and the Poynting flux integration box had dimensions 270 and 630 nm, respectively. We checked convergence by repeating some simulations on grids of $\Delta x = 2.5$ and $\Delta x = 1.25$ nm, and found that the time-averaged Poynting flux was well converged. The $\mathbf{J}(t) \cdot \mathbf{E}(t)$ method became unreliable at small grid sizes, as it becomes more sensitive to the pole in the Green function at the source point.

To confirm the accuracy of our calculations, we checked that our simulation method reproduced the analytic results of Chew [31] for the spontaneous emission rate of a dipole inside a sphere alone. Figure 7 shows a comparison of the analytic results and our FDTD calculations in the case of a dipole displaced by a factor of $0.6a$ from the centre with a grid size of $\Delta x = 5$ nm. Our results agree with the analytical calculations for $2a/\lambda \leqslant 0.5$, i.e. for wavelengths much shorter than those used in our main calculations, which correspond to the range indicated by the solid green bar. Similarly, we compared our FDTD method with the analytical result for the case of a dipole near a planar interface as shown in figure 1. The FDTD results (dashed lines) agree well with the semi-analytic theory (dots).

The simulations were performed for the diamond resting on the coverslip and for three different configurations on the opal: the diamond in the centre of the interstitial site; the diamond

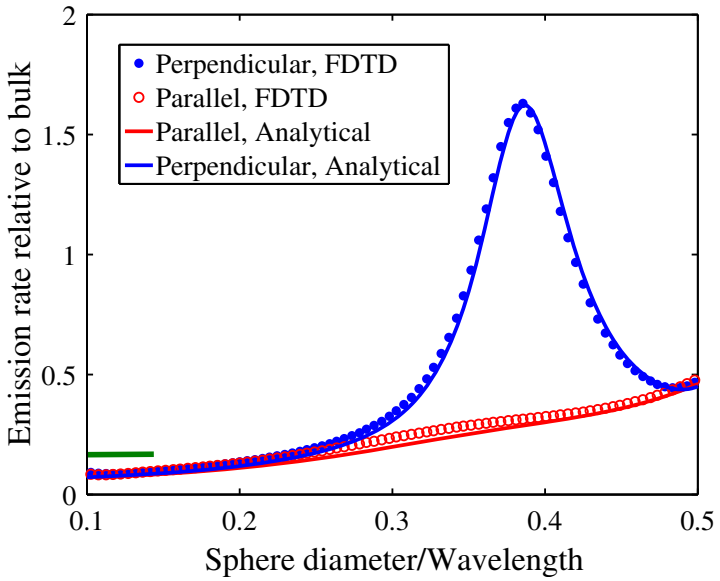

Figure 7. Comparison of emission rates, relative to that in bulk diamond, for a dipole inside an isolated diamond sphere calculated using FDTD and the analytical approach [31]. The dipole is positioned a distance $0.6a$ from the centre. Emission rates are shown for dipole orientations perpendicular and parallel to the radius vector of the dipole from the centre of the sphere. The solid green line corresponds to the size range of the nanodiamond crystals used in our experiments. The resonance for the perpendicular orientation corresponds to excitation of the lowest-order TE100 mode supported by the cavity.

resting halfway between the interstitial and the top of a sphere; and the diamond sitting on top of one sphere in the opal microstructure (see figure 4). The latter three positions were chosen on the basis of the SEM measurements discussed in section 3. The interstitial position was taken as the centre position between the three surrounding spheres with the diamond just spanning the gap between the adjacent beads. With variation in the diamond dimension, this position varies slightly, although the variation was found to have a less than 5% effect on the overall emission rate for a 10 nm fluctuation in diamond position. Similarly, a site halfway between the interstitial and top locations of opal sphere was taken to be representative of the distribution of intermediate locations. The small number of experimental samples and the resolution of the SEM measurements make a more precise comparison impossible.

4.2. Statistical averaging

For each of these four configurations, we need to average over the position and orientation of the dipole within each nanodiamond, since in our experiments we have no control over either variable. We assume that the dipole is uniformly distributed within the spherical nanodiamond (excluding a 5 nm surface shell) [52] and that the dipole orientation has no preferred direction, giving a total of five degrees of freedom. In calculations of emission rates for ideal systems, it is often possible to decompose the dependence on dipole orientation into emission due to dipole oscillation in two or three uncoupled perpendicular directions. This is true for both a dipole in a

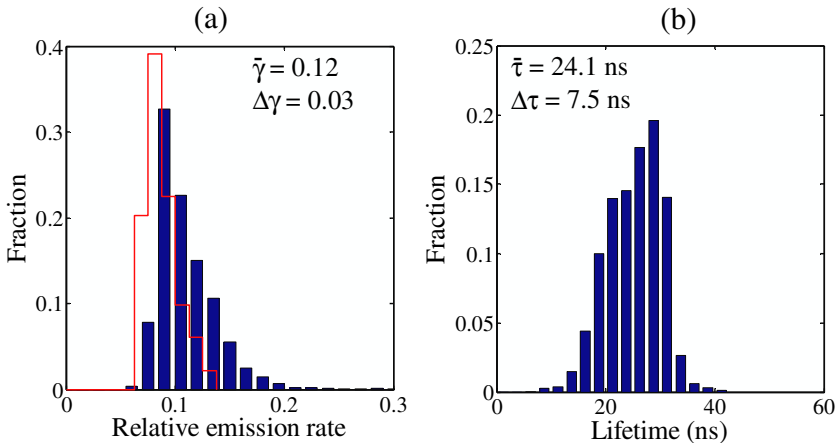

Figure 8. (a) Distribution of calculated FDTD (bars) and semi-analytical (red line) emission rates relative to bulk diamond rate for single NV centres on a coverslip. Quoted values are mean calculated (FDTD) emission rates $\bar{\gamma}$ and the range $\Delta\gamma$ that contains 50% of the centres. (b) Spontaneous emission lifetime distribution after scaling to the measured mean value.

sphere surrounded by a uniform medium [31] and for a dipole above a plane interface [40]. The overall emission rate is an angle weighted sum of the component rates. In general, however, due to low symmetry there can be coupling of the radiated electric field from one dipole orientation to the dipole motion in another. This is the case for our situation of a dipole inside a sphere, which itself is adjacent to a plane. The complete dependence on angle can then only be found by a sufficiently dense sampling of all directions on the unit sphere. Therefore, to completely characterize the expected distribution of emission rates we would need to perform a double average over all possible dipole positions and all possible dipole orientations at each position. Not only would this be a very large numerical undertaking, but also it seems excessive since our experiments involve ensembles of only around 30 observations and the experimental statistics are consequently quite noisy. Instead, to obtain a manageable number of simulations, we have constructed distributions of the lifetime by performing 1000 simulations with uniformly distributed random values of position and orientation for each of the four nanodiamond/substrate configurations. We find that this is sufficient to clearly capture the behaviour in each case. This averaging also accounts for the fact that NV is a 2D dipole and that for a fixed orientation it may radiate as a dipole oscillating in any direction perpendicular to the dipole axis. Averaging over this freedom is automatically included in the average over all dipole orientations.

4.3. Coverslip results and normalization

Figure 8(a) shows the FDTD calculated (bars) distribution of emission rates for the coverslip geometry relative to the rate Γ_b in bulk diamond. The mean calculated spontaneous emission rate is $R_C = 0.12R_b$, where the emission rate in bulk is $R_b = 1/11.6$ ns [18]. This corresponds to a predicted mean lifetime of $\bar{\tau} = 1/R_c = 96$ ns. The result shows a strong suppression in the emission rate as expected for a dipole enclosed within a dielectric sphere of size much smaller than the emission wavelength [31, 38, 43]. However, both the literature and our own measurements in figure 6(a) indicate that the experimentally measured mean lifetime of NV

centres in nanodiamonds on a coverslip is $\tau_{cov} \approx 20$–25 ns [18, 42, 53], which is a factor of 4 shorter than our calculated value.

Given this discrepancy, it is important to validate our calculations. Firstly, as described above, our computational approach reproduces the analytic results for the case of a dipole inside a dielectric sphere and for the case of a dipole near a flat dielectric interface. It involves the same code as the code that was used successfully in a large number of similar radiation dynamics problems [54–57]. To complement the FDTD calculations, we performed an additional calculation using a semi-analytical approach. Note that in the limit $a \leqslant \lambda$, the emission rate within an isolated sphere is very weakly dependent on the location of the dipole within the sphere [31]. Therefore, we can approximate the sphere–NV centre system as a point dipole with an intrinsic emission rate given by the bulk NV emission rate reduced by the local field factor in equation (5). We then use this effective dipole in the theory of Lukosz and Kunz [40] for the emission of a point dipole near a dielectric interface. We calculate the distribution of emission rates over all orientations of the dipole and for the range of positions it can take within the sphere. The results are shown by the red-line histogram in figure 8(a). While there is some discrepancy between the two models, which we attribute to the fact that the semi-analytic model ignores coupling between tangential and perpendicular field components that are present in the full model, this semi-analytical approach also predicts relative emission rates much lower than the experimental value of $\tau_{bulk}/\tau_{cov} \approx 0.5$.

We therefore conclude that electromagnetic LDOS effects alone are insufficient to account for the relationship between the measured lifetimes of NV centres in bulk diamond and NV in nanodiamonds at a planar surface. This difference may point to some other lifetime-reducing mechanism that has not yet been studied. Possibilities include a surface damage layer, unknown stress field, strongly non-spherical geometries or non-radiative processes. We return to this issue in section 5. Nevertheless, our discussion in section 2 shows that the agreement between the measured lifetime and the half-space volume averaging method of equation (4), which ignores all polarization effects and the embedding of the dipole in the nanoparticle, must be regarded as coincidental.

Given the considerable disagreement between the mean theoretical and experimental lifetimes, in the rest of this paper we simply concentrate on the relative change in lifetimes for the different substrates, and assume that an additional unknown factor gives rise to the absolute lifetime. To this end, the theoretical rates were linearly rescaled so that the calculated mean emission rate for the coverslip corresponds to the experimentally measured value of 24.1 ns. Figure 8(b) shows the distribution of emission lifetimes constructed from the scaled emission rates in figure 8(a). This scaling does not affect the polarization behaviour, which is the focus of this paper, as we used the same source of diamonds for both the coverslip and opal measurements and the same scaling is expected to apply.

4.4. Opal results

Figure 9 shows the calculated lifetime distributions for three indicative rest positions on the opal (interstitial, top and intermediate), as well as a weighted distribution (figure 9(d)) based on the probabilities to find crystals in any of the positions as measured by SEM. The weighted case shows a distinct shift to shorter lifetimes ($\bar{\tau} = 15.1$ ns) compared with the coverslip and consistent with the measured reduction of 29% in figure 6. Note that the distributions for each location are quite different. The mean lifetime for interstitial nanodiamonds (figure 9(a)) is a

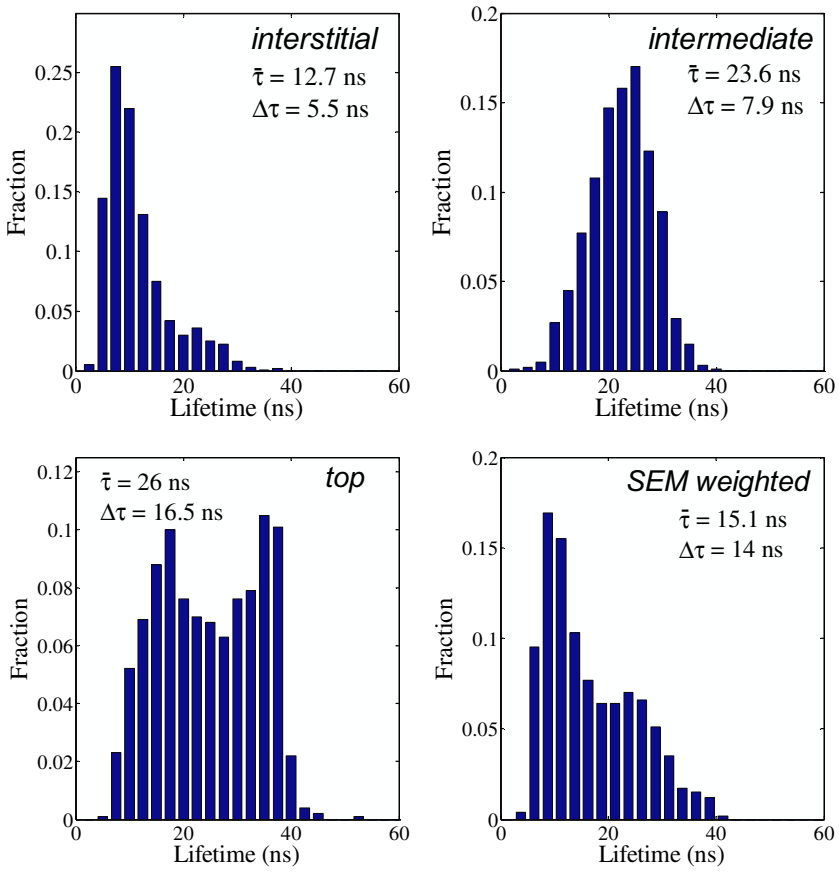

Figure 9. Relative emission lifetime distributions for single NV centres corresponding to various positions on an opal surface along with the overall weighted distribution. Here the weights are provided according to the statistical SEM measurements discussed in section 3.1. Each figure shows the mean of the distribution $\bar{\tau}$ and the range $\Delta\tau$ corresponding to 50% of the total centres.

factor of 2 smaller than that for nanodiamonds on the top of spheres (figure 9(c)). We can understand this significant change qualitatively with reference to the earlier discussion of dipole orientation. In particular, we attribute the reduction in lifetime to the multiple different interfaces of the local environment at the interstitial sites—almost all dipole directions have a component strongly perpendicular to one of the adjacent sphere surfaces. By analogy with the results in figure 1 for planar interfaces, we might expect that this quasi-perpendicular orientation leads to significant enhancement of the emission. In contrast, for nanodiamonds on the top of spheres, the supporting surface can be regarded as smooth with fairly low curvature and the distinction between parallel and perpendicular orientations remains strong. Note that the difference in emission rates cannot be accounted for merely by a change in the volume fraction f of high-index material (polystyrene) in the vicinity of the nanodiamond emitter. If we consider the region within a cubic wavelength of the emitter the volume fraction changes from $f = 0.36$ (sphere top) to $f = 0.46$ (interstitial site). From the calculation of expected lifetimes based only on an index-averaging model in figure 2, the reduction in lifetime would only be a factor of 0.04.

The same considerations also help us to account for the different relative distribution widths for each location in figure 9. For the interstitial and intermediate sites, the relative width $w = \Delta\tau/\bar{\tau}$ is $w = 0.43$ and $w = 0.33$, respectively. By contrast, for the sphere top site $w = 0.63$. The dependence of the emission rate on orientation is strongest for planar and near-planar structures, and is minimal for structures where different orientations are somewhat similar as is the case for the interstitial sites. When all possible directions are averaged over, the latter sites must show a weaker variation and therefore a narrower distribution.

5. Discussion

In this section, we consider several additional aspects of our modelling that might be contributing to the discrepancy between the predicted (96 ns) and measured (24 ns) lifetimes for diamonds on the coverslip.

Both the semi-analytic model and FDTD calculations do not account for any non-radiative component of the decay. In most of the published studies, the non-radiative component of NV decay is either ignored or considered to be small. Indeed, the quantum efficiency of NV in bulk diamond is known to be very close to 1 [58], and this is commonly considered [7, 29, 33, 59] to be the case for nanodiamonds of the size range studied in this work. Recently, it was found that for NV centres in 5 nm diamonds, the outer graphite shell of a few nanometres thickness constitutes a sufficient volume fraction of the crystal size to noticeably quench the emission [52]. A non-radiative component of decay with lifetime 15 ns was observed, in comparison with the radiative component at 25 ns. Given that in our case the diamonds are much larger and so the quenching effect due to surface graphite should be less pronounced, it seems very unlikely that this change could account for the factor of 4 discrepancy between measured and predicted lifetimes.

Several authors have accounted for observed lifetime reductions assuming close to perfect quantum efficiency. Using diamond crystals of similar sizes and assuming a quantum efficiency of 0.99, Schietinger *et al* [29] accounted for the achieved reduction in the overall lifetime of 7.5 and 9.5 times for two plasmonic configurations. The quenching due to gold nanoparticles only reduced the quantum efficiency to 0.78. Ruijgrok *et al* [33], also using similar sized crystals, were able to demonstrate the effect of the environment on the emission lifetime of the same set of NV emitters using dielectric spheres with the change in lifetime attributed to a change in the LDOS corresponding to radiative emission. Thus, currently, there does not seem to be a candidate non-radiative decay mechanism that can account for the lifetime discrepancy.

Our modelling does not include the variation in crystal size—we performed simulations for a fixed nanodiamond diameter of 54 nm. However, the size variation of the actual nanodiamonds used (discussed in section 3.1) corresponds to the range of $2a/\lambda$ indicated by the green bar in figure 7. Over this range, we see that the emission curve for the sphere alone is almost perfectly flat. Thus, we expect that the variation in emission rate in the full system due to nanodiamond size should be a very weak effect.

To ensure that our calculated distributions of the emission rate were not peculiar to the choice of spherical nanodiamonds, we performed additional FDTD calculations for a variety of nanodiamonds of different shapes supported by the coverslip substrate. The results are shown in figure 10. We considered a sphere of diameter 60 nm, an octahedron of side length 60 nm resting on a vertex, a cube of side length 60 nm resting on a face and two oblate ellipsoids with semi-axis lengths $(a\eta,\ a\eta,\ a/\eta^2)$ for $\eta = 1.2$ and 1.4. Despite the variety of shapes, the distributions

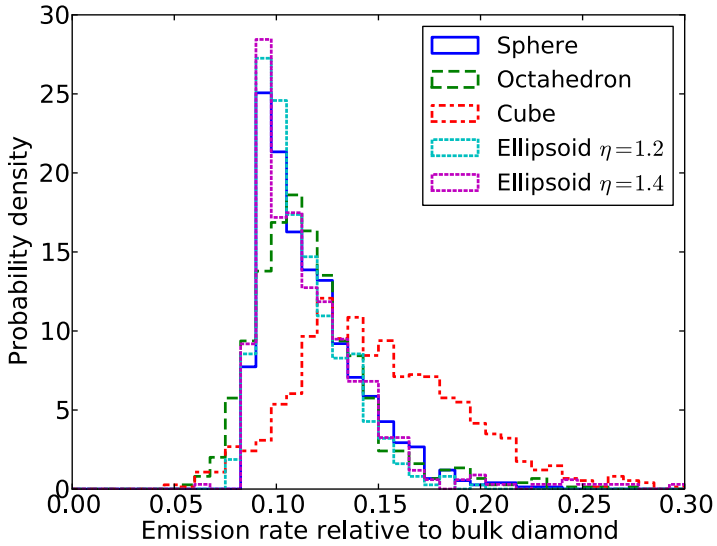

Figure 10. Relative emission rates for nanodiamonds of various idealized shapes on a glass substrate.

are remarkably similar. The cube shows a significantly broader distribution than the others, because there is a clear distinction between parallel and perpendicular alignment of dipoles that lie close to one of the faces of the cube. For the other shapes, the distinction between parallel and perpendicular orientations is less clear, and the distribution widths are narrower. However, even allowing for the cube case, it is clear that the mean rate and width of the distributions are generic properties of nanodiamonds of this scale and the results in section 4 are not restricted to spherical diamonds alone. While our actual diamonds are not true spheres, figure 10 suggests that they would require extreme profiles in order to increase the emission rate by a factor of 4, and this is not supported by SEM analysis.

Another potential cause of the measured enhancement substantially exceeding the predicted rate might be the enhancement through coupling to guided wave slab modes in the substrate. However, with a coverslip thickness of $\sim$150 μm, it seems reasonable to treat the substrate as a semi-infinite bulk medium as we have done here.

6. Conclusion

Gaining a quantitative understanding of the behaviour of single dipole emitters in and around a variety of materials and structures underpins practical single-photon device development. We have presented detailed measurements of single-photon emission lifetimes for NV centres in nanodiamonds on flat and structured surfaces. The dipole orientation relative to the surfaces around it plays an important role, and the emission rate varies significantly depending on this. We have established that there is a clear difference in lifetime between crystals randomly distributed on a flat surface and crystals randomly distributed on structured opal surfaces. The experimentally measured single-photon emission rates for diamond on the opal show a factor of 1.5 average enhancement compared with the coverslip case. This result is supported by a rigorous FDTD model which indicates that the primary reason for the enhancement is the dipole orientation with respect to the local surface. A comparison of calculations with experiments not

only clarifies the interaction of an optical dipole in diamond with a surface, but also provides new insights into the physical system which are yet to be understood, including the large discrepancy between measured and predicted absolute lifetimes of NV centres in nanodiamonds. These discrepancies only emerge when the embedding of the dipole in the nanodiamond is explicitly taken into account. In summary, we have presented a comprehensive theoretical model and experimental measurements of enhanced spontaneous emission rates of single NV centres in diamond. In addition to the fundamental physical interest, this work hints at a realistic avenue for the development of nanodiamond-based probes to measure the electromagnetic density of states in complex nano/microstructured materials or devices. Coupled with new advances in fabrication and nanoassembly, this work adds a valuable resource for the development of a range of photonic devices.

References

[1] Lounis B and Moerner W E 2000 Single photons on demand from a single molecule at room temperature *Nature* **407** 491–3

[2] Sanders B, Vuckovic J and Grangier P 2005 Single photons on demand *Europhys. News* **36** 56–8

[3] Scheel S 2009 Single-photon sources—an introduction *J. Mod. Opt.* **56** 141–60

[4] Lounis B and Orrit M 2005 Single-photon sources *Rep. Prog. Phys.* **68** 1129–79

[5] Oxborrow M and Sinclair A G 2005 Single-photon sources *Contemp. Phys.* **46** 173–206

[6] Park Y S, Cook A K and Wang H L 2006 Cavity QED with diamond nanocrystals and silica microspheres *Nano Lett.* **6** 2075–9

[7] Schietinger S and Benson O 2009 Coupling single NV-centres to high-Q whispering gallery modes of a preselected frequency-matched microresonator *J. Phys. B: At. Mol. Opt. Phys.* **42** 114001

[8] Santori C, Barclay P E, Fu K M C, Beausoleil R G, Spillane S and Fisch M 2010 Nanophotonics for quantum optics using nitrogen-vacancy centers in diamond *Nanotechnology* **21** 274008

[9] Stewart L A, Zhai Y, Dawes J M, Steel M J, Rabeau J R and Withford M J 2009 Single photon emission from diamond nanocrystals in an opal photonic *Cryst. Opt. Express* **17** 18044–53

[10] Wolters J, Schell A W, Kewes G, Nusse N, Schoengen M, Doscher H, Hannappel T, Lochel B, Barth M and Benson O 2010 Enhancement of the zero phonon line emission from a single NV-center in a nanodiamond via coupling to a photonic crystal cavity *Appl. Phys. Lett.* **97** 141108

[11] Van der Sar T, Hagemeier J, Pfaff W, Heeres E C, Thon S M, Kim H, Petroff P M, Oosterkamp T H, Bouwmeester D and Hanson R 2011 Deterministic nanoassembly of a coupled quantum emitter–photonic crystal cavity system *Appl. Phys. Lett.* **98** 193103

[12] Englund D, Shields B, Rivoire K, Hatami F, Vuckovic J, Park H and Lukin M D 2010 Deterministic coupling of a single nitrogen vacancy center to a photonic crystal cavity *Nano Lett.* **10** 3922–6

[13] Purcell E M, Torrey H C and Pound R V 1946 Resonance absorption by nuclear magnetic moments in a solid *Phys. Rev.* **69** 37

[14] Boroditsky M, Vrijen R, Krauss T F, Coccioli R, Bhat R and Yablonovitch E 1999 Spontaneous emission extraction and Purcell enhancement from thin-film 2-D photonic crystals *J. Lightwave Technol.* **17** 2096–112

[15] Schroder T, Gadeke F, Banholzer M J and Benson O 2011 Ultrabright and efficient single-photon generation based on nitrogen-vacancy centres in nanodiamonds on a solid immersion lens *New J. Phys.* **13** 055017

[16] Castelletto S *et al* 2011 Diamond-based structures to collect and guide light *New J. Phys.* **13** 025020

[17] Rabeau J R, Stacey A, Rabeau A, Prawer S, Jelezko F, Mirza I and Wrachtrup J 2007 Single nitrogen vacancy centers in chemical vapor deposited diamond nanocrystals *Nano Lett.* **7** 3433–7

[18] Kurtsiefer C, Mayer S, Zarda P and Weinfurter H 2000 Stable solid-state source of single photons *Phys. Rev. Lett.* **85** 290–3

[19] Tamarat P *et al* 2006 Stark shift control of single optical centers in diamond *Phys. Rev. Lett.* **97** 083002
[20] Orwa J O, Aharonovich I, Jelezko F, Balasubramanian G, Balog P, Markham M, Twitchen D J, Greentree A D and Prawer S 2010 Nickel related optical centres in diamond created by ion implantation *J. Appl. Phys.* **107** 093512
[21] Gaebel T, Popa I, Gruber A, Domhan M, Jelezko F and Wrachtrup J 2004 Stable single-photon source in the near infrared *New J. Phys.* **6** 98
[22] Wu E, Rabeau J R, Roger G, Treussart F, Zeng H, Grangier P, Prawer S and Roch J F 2007 Room temperature triggered single-photon source in the near infrared *New J. Phys.* **9** 434
[23] Rabeau J R, Chin Y L, Prawer S, Jelezko F, Gaebel T and Wrachtrup J 2005 Fabrication of single nickel-nitrogen defects in diamond by chemical vapor deposition *Appl. Phys. Lett.* **86** 131926
[24] Marshall G D, Gaebel T, Mathews J C F, Enderlein J, O'Brein J L and Rabeau J 2011 Coherence properties of a single dipole emitter in diamond *New J. Phys.* **13** 055016
[25] Aharonovich I, Castelletto S, Simpson D A, Stacey A, McCallum J, Greentree A D and Prawer S 2009 Two-level ultrabright single photon emission from diamond nanocrystals *Nano Lett.* **9** 3191–5
[26] Aharonovich I, Castelletto S, Johnson B C, McCallum J C, Simpson D A, Greentree A D and Prawer S 2010 Chromium single-photon emitters in diamond fabricated by ion implantation *Phys. Rev.* B **81** 121201
[27] Aharonovich I, Castelletto S, Simpson D A, Greentree A D and Prawer S 2010 Photophysics of chromium-related diamond single-photon emitters *Phys. Rev.* A **81** 043813
[28] Elke N *et al* 2011 Single photon emission from silicon-vacancy colour centres in chemical vapour deposition nano-diamonds on iridium *New J. Phys.* **13** 025012
[29] Schietinger S, Barth M, Alchele T and Benson O 2009 Plasmon-enhanced single photon emission from a nanoassembled metal–diamond hybrid structure at room temperature *Nano Lett.* **9** 1694–8
[30] Kolesov R, Grotz B, Balasubramanian G, Stohr R J, Nicolet A A L, Hemmer P R, Jelezko F and Wrachtrup J 2009 Wave–particle duality of single surface plasmon polaritons *Nat. Phys.* **5** 470–4
[31] Chew H 1988 Radiation and lifetimes of atoms inside dielectric particles *Phys. Rev.* A **38** 3410
[32] Lee K G, Chen X W, Eghlidi H, Kukura P, Lettow R, Renn A, Sandoghdar V and Gotzinger S 2011 A planar dielectric antenna for directional single-photon emission and near-unity collection efficiency *Nat. Photonics* **5** 166–9
[33] Ruijgrok P V, Wuest R, Rebane A A, Renn A and Sandoghdar V 2010 Spontaneous emission of a nanoscopic emitter in a strongly scattering disordered medium *Opt. Express* **18** 6360–5
[34] Glauber R J and Lewenstein M 1991 Quantum optics of dielectric media *Phys. Rev.* A **43** 467
[35] Koenderink A F, Kafesaki M, Soukoulis C M and Sandoghdar V 2006 Spontaneous emission rates of dipoles in photonic crystal membranes *J. Opt. Soc. Am. B: Opt. Phys.* **23** 1196–206
[36] Xu Y, Vuckovic J S, Lee R K, Painter O J, Scherer A and Yariv A 1999 Finite-difference time-domain calculation of spontaneous emission lifetime in a microcavity *J. Opt. Soc. Am. B: Opt. Phys.* **16** 465–74
[37] Stephen M B *et al* 1996 Decay of excited atoms in absorbing dielectrics *J. Phys. B: At. Mol. Opt. Phys.* **29** 3763
[38] Kien F L, Quang N H and Hakuta K 2000 Spontaneous emission from an atom inside a dielectric sphere *Opt. Commun.* **178** 151–64
[39] Rogobete L, Schniepp H, Sandoghdar V and Henkel C 2003 Spontaneous emission in nanoscopic dielectric particles *Opt. Lett.* **28** 1736–8
[40] Lukosz W and Kunz R E 1977 Light-emission by magnetic and electric dipoles close to a plane interface. 1. Total radiated power *J. Opt. Soc. Am.* **67** 1607–15
[41] Kreiter M, Prummer M, Hecht B and Wild U P 2002 Orientation dependence of fluorescence lifetimes near an interface *J. Chem. Phys.* **117** 9430–3
[42] Beveratos A, Brouri R, Gacoin T, Poizat J P and Grangier P 2001 Nonclassical radiation from diamond nanocrystals *Phys. Rev.* A **64** 061802
[43] Schniepp H and Sandoghdar V 2002 Spontaneous emission of europium ions embedded in dielectric nanospheres *Phys. Rev. Lett.* **89** 257403

[44] Wubs M, Suttorp L G and Lagendijk A 2003 Multipole interaction between atoms and their photonic environment *Phys. Rev.* A **68** 13822
[45] Pukhov K K, Basiev T T and Orlovskii Y V 2008 Spontaneous emission in dielectric nanoparticles *J. Exp. Theor. Phys. Lett.* **88** 12–8
[46] Eckert A 1997 *The World of Opals* (New York: Wiley)
[47] Sanders J V 1964 Colour of precious opal *Nature* **204** 1151–3
[48] Jiang P, Bertone J F, Hwang K S and Colvin V L 1999 Single-crystal colloidal multilayers of controlled thickness *Chem. Mater.* **11** 2132–40
[49] Bradac C, Gaebel T, Naidoo N, Rabeau J R and Barnard A S 2009 Prediction and measurement of the size-dependent stability of fluorescence in diamond over the entire nanoscale *Nano Lett.* **9** 3555–64
[50] Bradac C, Gaebel T, Naidoo N, Sellars M J, Twamley J, Brown L J, Barnard AS, Plakhotnik T, Zvyagin A V and Rabeau J R 2010 Observation and control of blinking nitrogen-vacancy centres in discrete nanodiamonds *Nat. Nanotechnol.* **5** 345–9
[51] Press W H, Teukolsky S A, Vetterling W T and Flannery B P 2007 *Numerical Recipes: The Art of Scientific Computing* 3rd edn (Cambridge: Cambridge University Press)
[52] Smith B R, Gruber D and Plakhotnik T 2009 The effects of surface oxidation on luminescence of nano diamonds *Diam. Relat. Mater.* **19** 314–8
[53] Tisler J *et al* 2009 Fluorescence and spin properties of defects in single digit nanodiamonds *ACS Nano* **3** 1959–65
[54] Tomljenovic-Hanic S, Steel M J, de, Sterke C M and Moss D J 2007 High-Q cavities in photosensitive photonic crystals *Opt. Lett.* **32** 542–4
[55] Bordas F, Steel M J, Seassal C and Rahmani A 2007 Confinement of band-edge modes in a photonic crystal slab *Opt. Express* **15** 10890–902
[56] Bordas F, Seassal C, Dupuy E, Regreny P, Gendry M, Viktorovitch P, Steel M J and Rahmani A 2009 Room temperature low-threshold InAs/InP quantum dot single mode photonic crystal microlasers at 1.5 μm using cavity-confined slow light *Opt. Express* **17** 5439–45
[57] Tomljenovic-Hanic S, Steel M J, de Sterke C M and Salzman J 2006 Diamond-based photonic crystal microcavities *Opt. Express* **14** 3556–62
[58] Gruber A, Dräbenstedt A, Tietz C, Fleury L, Wrachtrup J and Borczyskowski C V 1997 Scanning confocal optical microscopy and magnetic resonance on single defect centers *Science* **276** 2012–4
[59] Gaebel T *et al* 2006 Photochromism in single nitrogen-vacancy defect in diamond *Appl. Phys. B: Lasers Opt.* **82** 243–6